



# Ultrafast charge transfer in a type-II MoS<sub>2</sub>-ReSe<sub>2</sub> van der Waals heterostructure

LU ZHANG,<sup>1</sup> DAWEI HE,<sup>1</sup> JIAQI HE,<sup>1,\*</sup> YANG FU,<sup>1</sup> ANG BIAN,<sup>1</sup> XIUXIU HAN,<sup>1</sup> SHUANGYAN LIU,<sup>1</sup> YONGSHENG WANG,<sup>1,3</sup> AND HUI ZHAO<sup>2</sup>

<sup>1</sup>Key Laboratory of Luminescence and Optical Information, Ministry of education, Institute of Optoelectronic Technology, Beijing Jiaotong University, Beijing 100044, China

<sup>2</sup>Department of Physics and Astronomy, The University of Kansas, Lawrence, Kansas 66045, USA

<sup>3</sup>yshwang@bjtu.edu.cn

\*jqhe@bjtu.edu.cn

**Abstract:** We fabricated a van der Waals heterostructure by stacking together monolayers of MoS<sub>2</sub> and ReSe<sub>2</sub>. Transient absorption measurements were performed to study the dynamics of charge transfer, indirect exciton formation, and indirect exciton recombination. The results show that the heterostructure form a type-II band alignment with the conduction band minimum and valance band maximum located in the MoS<sub>2</sub> and ReSe<sub>2</sub> layers, respectively. By using different pump-probe configurations, we found that electrons could efficiently transfer from ReSe<sub>2</sub> to MoS<sub>2</sub> and holes along the opposite direction. Once transferred, the electrons and holes form spatially indirect excitons, which have longer recombination lifetimes than excitons in individual monolayers. These results provide useful information for developing van der Waals heterostructure involving ReSe<sub>2</sub> for novel electronic and optoelectronic applications.

© 2019 Optical Society of America under the terms of the [OSA Open Access Publishing Agreement](#)

## 1. Introduction

The discovery of graphene in 2004 [1] has stimulated intensive research on a broad range of two-dimensional (2D) materials, among which layered transition metal dichalcogenides (TMDs) have attracted much attention. Most monolayer TMDs studied so far has a direct bandgap and thickness-dependent bandgaps. Their ultrathin thickness and superior electronic and optical properties make them promising materials for optoelectronic and electronic devices such as photodetectors [2–4], solar cells [5–7] and integrated circuits [8–10].

Among the semiconductors in the family of TMDs, MoS<sub>2</sub> has attracted the most attention. Bulk MoS<sub>2</sub> exhibits an indirect bandgap of about 1.2 eV, while its monolayer form is direct-gap semiconductor with a bandgap of about 1.8 eV [11,12]. ReSe<sub>2</sub> is another representative semiconducting TMDs. Theoretical calculations showed that ReSe<sub>2</sub> lacks the indirect-to-direct bandgap transition often observed in TMDs [13–16]. It remains an indirect semiconductor from bulk to monolayer forms. Optical spectroscopic measurements indicated that its bandgap increases from 1.26 eV in the bulk to 1.32 eV in the monolayer at 80 K [13]. Monolayer layer ReSe<sub>2</sub> transistors have been fabricated, with high mobility and high photoresponsivity [15]. The excitons are strongly polarized with dipole vectors along different crystal directions, which persist from bulk down to monolayer thickness, as shown by polarization-resolved photoluminescence and transmission spectroscopy [17]. Unlike most TMDs with the 2H lattice structure (such as MoS<sub>2</sub>, MoSe<sub>2</sub>, WS<sub>2</sub>, and WSe<sub>2</sub>), ReSe<sub>2</sub> crystals exhibit a distorted 1T lattice structure [15]. Owing to this lattice structure, ReSe<sub>2</sub> exhibits strong in-plane anisotropic optical, electronic, and mechanical properties [18–21].

Another research topic of great current interests associated with 2D materials is to develop van der Waals heterostructures by stacking together different monolayers. Since the van der Waals interlayer coupling does not require lattice matching of the component materials, this approach can produce a vast number of new materials [22]. In order to harness desired

properties, different combinations of 2D materials have been designed and fabricated to tune the electrical and optical properties of the materials [23–30]. So far, combinations of the most common TMDs materials, such as MoS<sub>2</sub>, MoSe<sub>2</sub>, WS<sub>2</sub>, and WSe<sub>2</sub>, have been the main focus. The charge transfer properties in these heterostructure have been studied by transient absorption measurements [31–34]. However, the charge transfer in heterostructure involving ReSe<sub>2</sub> has not been investigated so far.

In this work, we fabricated a van der Waals heterostructure by stacking together monolayers of MoS<sub>2</sub> and ReSe<sub>2</sub>. Transient absorption measurements were performed to study the dynamics of charge transfer, indirect exciton formation, and indirect exciton recombination. We found evidence of the type-II nature of this heterostructure, which facilitates the transfer of electrons from ReSe<sub>2</sub> to MoS<sub>2</sub> and holes along the opposite direction. When transferred, electrons and holes form spatially indirect excitons with longer recombination lifetimes than the excitons in individual monolayers. These results provide useful information for developing van der Waals heterostructures using ReSe<sub>2</sub>.

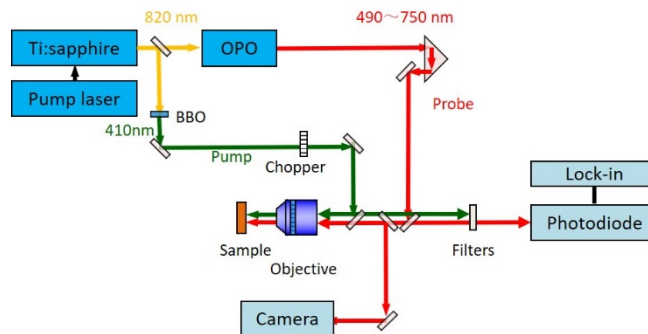


Fig. 1. Schematics of the differential reflection setup.

## 2. Experimental

Monolayer ReSe<sub>2</sub> films were acquired from 6 Carbon Technology Corporation. The films were fabricated by chemical vapor deposition (CVD) and then transferred to a silicon substrate, which is covered by a 300-nm thermally grown SiO<sub>2</sub> layer. Two monolayer MoS<sub>2</sub> flakes were obtained by micromechanical exfoliation of a bulk crystal onto polydimethylsiloxane (PDMS) substrates using adhesive tapes. One of them was transferred onto the ReSe<sub>2</sub> film, another onto another Si/SiO<sub>2</sub> substrate. The samples were annealed at 200 °C for 2 h in an Ar environment at a base pressure of about 5 Torr. Because the ReSe<sub>2</sub> is a polycrystalline film, the relative crystalline orientation between MoS<sub>2</sub> and ReSe<sub>2</sub> is unknown.

The photocarrier dynamics in the MoS<sub>2</sub>-ReSe<sub>2</sub> heterostructure and the monolayers of MoS<sub>2</sub> and ReSe<sub>2</sub> was studied by a transient absorption technique [35]. Figure 1 shows schematically the differential reflection setup used in this study. An 80-MHz mode-locked Ti:sapphire laser generates 100 fs pulses with a central wavelength of 820 nm. This pulse was divided to two parts by a beamsplitter. One part was used to pump an optical parametric oscillator to generate a signal output with a central wavelength in the range of 490-750 nm. The other part was used directly or focused to a beta barium borate crystal to generate its second harmonic at 410 nm. Different combinations of these three pulses were used as pump and probe pulses according to the measurement goals. The pump and probe beams were combined with a beamsplitter and focused to the sample surface through a microscope objective lens. The reflected beam was detected by a silicon photodiode. Color filters were used to prevent the unwanted light from reaching the photodiode. A lock-in amplifier was used to measure the voltage output of the photodiode. A mechanical chopper was placed at the pump path to modulate its intensity at 2 KHz. The voltage detected by the lock-in

amplifier synchronized to the chopper is proportional to the differential reflection of the probe,  $\Delta R/R_0 = (R-R_0)/R_0$ , where  $R$  and  $R_0$  are the reflection coefficients of the sample at the probe wavelength with the pump presence and without it, respectively. The differential reflection was measured as a function of the probe delay, which is defined as the difference of the arrival times of the probe and pump pulses at the sample. This was achieved by controlling the path length of the pump pulse with a linear motor stage. All the measurements were performed with the samples under ambient condition.

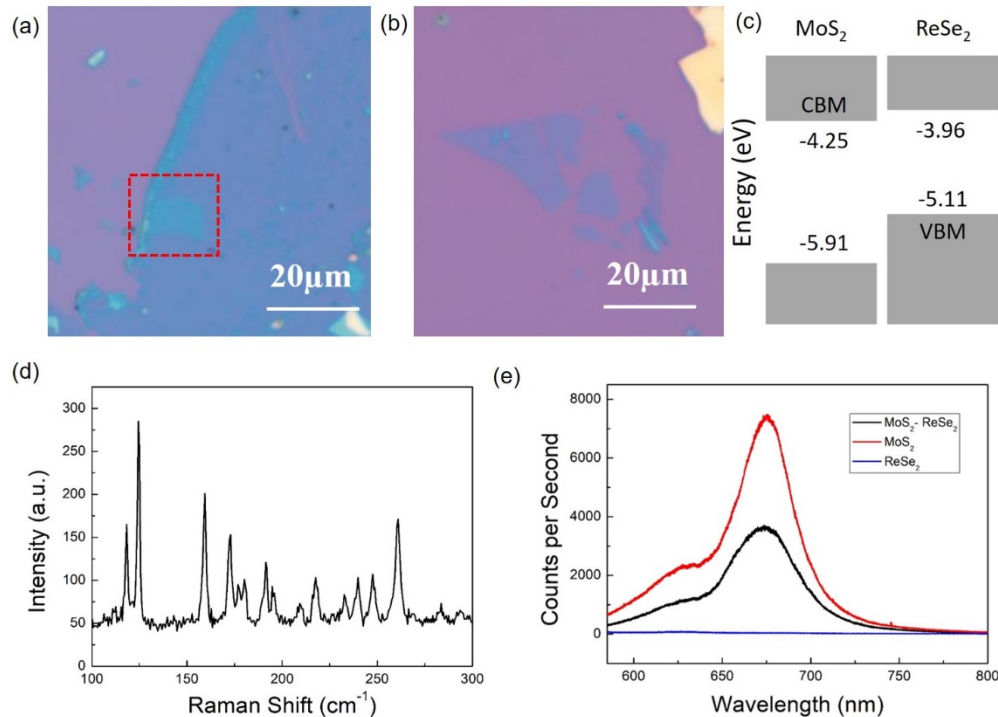


Fig. 2. (a) Optical microscope image of the ReSe<sub>2</sub> film and MoS<sub>2</sub>-ReSe<sub>2</sub> heterostructure, the heterostructure is in the red dashed box. (b) Optical microscope image of the monolayer MoS<sub>2</sub> flake. (c) The predicted band alignment of the MoS<sub>2</sub>-ReSe<sub>2</sub> heterostructure. The numbers are the energy differences from the vacuum level (in electron volts) according to the calculation. (d) Photoluminescence spectra of the samples.

### 3. Results and discussion

Figure 2(a) shows an optical microscope image of the monolayer ReSe<sub>2</sub> film and the MoS<sub>2</sub>-ReSe<sub>2</sub> heterostructure on a Si/SiO<sub>2</sub> substrate. The other monolayer MoS<sub>2</sub> flake on a separated substrate is shown in Fig. 2(b). According to the predicted band alignment of this heterostructure [36], as shown in Fig. 2(c), MoS<sub>2</sub> and ReSe<sub>2</sub> form a type-II band alignment with the conduction band minimum (CBM) and valence band maximum (VBM) located in the MoS<sub>2</sub> and ReSe<sub>2</sub> layers, respectively. Note that in this calculation [36] the interlayer coupling was not included. The band alignment was determined directly from the electron affinity and ionization potential of individual monolayers of MoS<sub>2</sub> and ReSe<sub>2</sub> (which are labeled in the figure in the unit of eV). Due to this limitation, no values of the band offset are adopted. Figure 2(d) shows the Raman spectrum of the monolayers ReSe<sub>2</sub> film. The monolayer ReSe<sub>2</sub> have 18 potential Raman modes due to the presence of 12 atoms in each unit cell of the ReSe<sub>2</sub> crystal lattice [14]. There more than 10 distinctive Raman peaks have been detected in the Raman spectrum of monolayer ReSe<sub>2</sub> film. Raman peak at 125 cm<sup>-1</sup> is observed and assigned to the E<sub>g</sub>-like, as the vibration is mostly in-plane and symmetric [13].

The peaks located at 160 and 173  $\text{cm}^{-1}$  are ascribed as  $A_g$ -like modes since the main vibrations are in the one-dimensional vertical direction [13].

Figure 2(e) shows the photoluminescence (PL) spectra measured from the  $\text{MoS}_2$ ,  $\text{ReSe}_2$ , and the  $\text{MoS}_2$ - $\text{ReSe}_2$  heterostructure regions under the excitation of a 532-nm continuous-wave laser. The PL yield and the spectral shape of  $\text{MoS}_2$  are both consistent with previously reported results of monolayer  $\text{MoS}_2$  [37]. With the same experimental conditions,  $\text{ReSe}_2$  film shows no detectable PL in this spectral range. For the heterostructure region, the PL peak position is close to that of  $\text{MoS}_2$ . This suggests that the optical bandgap of the  $\text{MoS}_2$  layer is almost unchanged in the heterostructure. The peak height of the heterostructure is about 50% of that of the individual  $\text{MoS}_2$  monolayer. This quenching of the  $\text{MoS}_2$  peak is indicative of charge or energy transfer from  $\text{MoS}_2$  to  $\text{ReSe}_2$ . The small quenching factor is consistent with results from other heterostructures involving  $\text{MoS}_2$  [32], and can be attributed to the short exciton lifetime in this material. We also note that the PL from the heterostructure is slightly broader than monolayer  $\text{MoS}_2$ , which could be due to additional scattering of excitons introduced by defects in  $\text{ReSe}_2$ . However, more studies are needed to fully understand this feature.

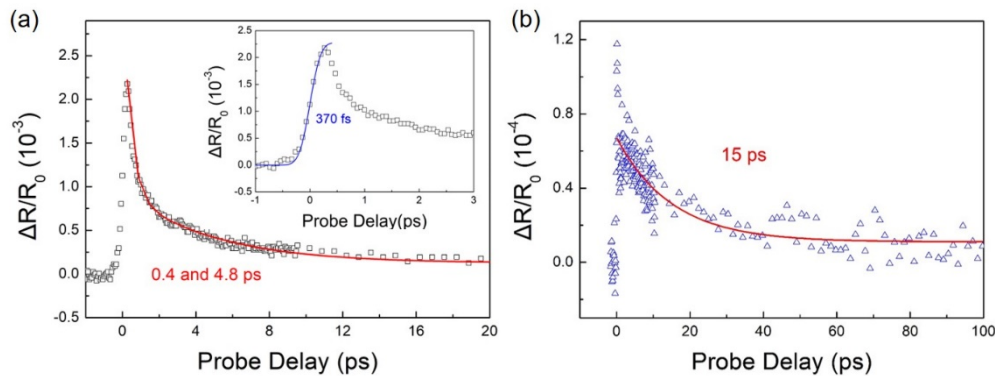


Fig. 3. Photocarrier dynamics in individual monolayers. (a) Differential reflection signal of monolayer  $\text{MoS}_2$  measured with a 410 nm pump and a 672 nm probe pulses. The red line is a fit by a bi-exponential function. The inset provides a closer look at the data near zero probe delay. (b) Differential reflection signals of monolayer  $\text{ReSe}_2$  measured with a 672 nm pump and an 820 nm probe pulses. The red line is a fit by an exponential function.

In the transient absorption measurements, we first investigated the individual monolayers of  $\text{MoS}_2$  and  $\text{ReSe}_2$  samples. Figure 3(a) shows the differential reflection signal of  $\text{MoS}_2$ . In this measurement, a 410 nm pump pulse with a fluence of  $5.6 \mu\text{J cm}^{-2}$  was used to inject photocarriers in the sample. A 672 nm probe pulse was used to study their temporal dynamics. The rise of the signal can be fit by the integral of a Gaussian function with a full width at half maximum of 370 fs, as indicated by the blue curve over the data points in the inset of Fig. 3(a). The decay of the signal can be fit by a bi-exponential function, as indicated by the red line in Fig. 3(a), with a short and long time constant of about 0.4 and 4.8 ps, respectively. By repeating the measurement with other pump fluences, we found that the decay time constants are independent of the pump fluence while the magnitude increases linearly with the fluence. The short time constant can be attributed to the exciton formation process, based on previous studies [38,39]. The long time constant reflects the recombination lifetime of the excitons [35]. This relatively short lifetime is controlled by nonradiative recombination of excitons. Figure 3(b) shows the differential reflection signal from the monolayer  $\text{ReSe}_2$ . A 672 nm pulses with a peak fluence of  $76 \mu\text{J cm}^{-2}$  and an 820 nm pulses were used as the pump and probe, respectively. The decay of the signal can be fit by a single exponential function, as indicated by the red line, with a time constant of about 15 ps. Similarly, this time constant is attributed to the nonradiative recombination lifetime in  $\text{ReSe}_2$ .

We note that due to the relatively low signal-to-noise ratio of  $\text{ReSe}_2$ , no multiple exponential fits were attempted.

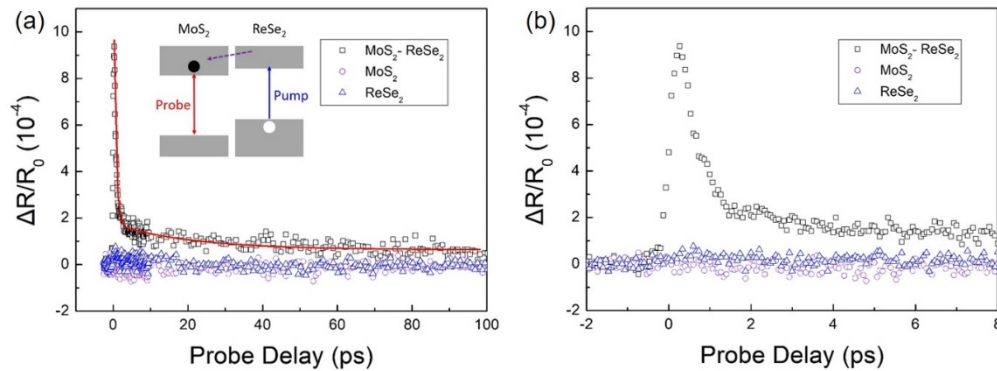


Fig. 4. Electron transfer from  $\text{ReSe}_2$  to  $\text{MoS}_2$ . (a) Black squares show the differential reflection signal from the  $\text{MoS}_2$ - $\text{ReSe}_2$  heterostructure sample with an 820 nm pump and a 672 nm probe pulses. The red line is a fit. The purple circles and the blue triangles are signals from the  $\text{MoS}_2$  and  $\text{ReSe}_2$  monolayer samples under the same conditions, respectively, showing lack of signal from these samples, as expected. (b) Same as (a) but over a shorter time range to show the initial dynamics.

Next, we performed transient absorption measurements with different pump-probe configurations to study the  $\text{MoS}_2$ - $\text{ReSe}_2$  heterostructure. We first studied the electron transfer from  $\text{ReSe}_2$  to  $\text{MoS}_2$ , with a pump-probe configuration shown in the inset of Fig. 4(a). We selectively excite electrons in  $\text{ReSe}_2$  with an 820 nm pump pulse (blue vertical arrow). The pump photon energy is not enough to excite the  $\text{MoS}_2$  layer, which has an optical bandgap of 1.85 eV. After being excited, the electrons in  $\text{ReSe}_2$  are expected to transfer to  $\text{MoS}_2$  across the van der Waals interface (violet dashed arrow). A 672 nm probe pulse is tuned to the optical bandgap of the  $\text{MoS}_2$  to monitor the electron transfer process (red vertical arrow). The black symbols in Figs. 4(a) and 4(b) show the obtained signal on long and short time ranges, respectively, with a pump pulse fluence of  $22 \mu\text{J cm}^{-2}$ . For comparison, no signal was observed from the two monolayer samples, as shown by the purple circles and blue triangles. The lack of signal from these two samples are expected: For  $\text{MoS}_2$ , the pump pulse has no sufficient energy to excite carriers, while for  $\text{ReSe}_2$ , the probe photon energy is too high compared to its bandgap to effectively detect carriers. Hence, the signal from the heterostructure can only be attributed to the electrons that are excited in  $\text{ReSe}_2$  and sequentially transferred to  $\text{MoS}_2$ . We found that the signal reaches a peak on an ultrashort time scale, which is limited by the time resolution of this measurement. This indicates that the electron transfer is a sub-100 fs process. The decay of the signal can be fit by bi-exponential function, as indicated by the red line in Fig. 4(a), with the short and long time constants of about 0.5 and 21 ps, respectively. The long time constant reflects that the lifetime of the transferred electrons in  $\text{MoS}_2$  is about 4 times longer than the exciton lifetime in monolayer  $\text{MoS}_2$ , due to the charge separation: Since electrons and holes populate the  $\text{MoS}_2$  and  $\text{ReSe}_2$  layers, respectively, their recombination is suppressed. The short time constant could be attributed to the formation of indirect exciton of electrons in  $\text{MoS}_2$  and holes in  $\text{ReSe}_2$ .

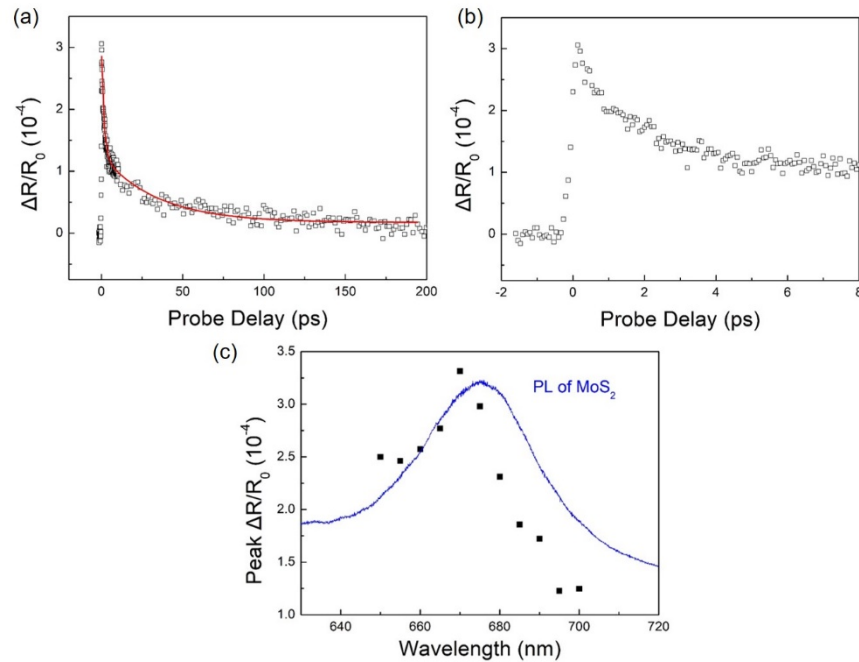


Fig. 5. Hole transfer from MoS<sub>2</sub> to ReSe<sub>2</sub>. (a) Differential reflection signals of the heterostructure sample measured with a 672 nm pump and an 820 nm probe pulses. The red line is a fit by an exponential function. (b) The same as (a) but in a shorter time range. (c) Peak differential reflection signal from the heterostructure as a function of the pump wavelength (black squares) and the PL spectrum of the MoS<sub>2</sub> (blue curve).

Since the bandgap of ReS<sub>2</sub> is smaller than MoS<sub>2</sub>, the observation of electron transfer from ReS<sub>2</sub> to MoS<sub>2</sub> indicates the band alignment is type-II, with the CBM and VBM located in the MoS<sub>2</sub> and ReS<sub>2</sub> layers, respectively, which is consistent with theory. Such an alignment should allow transfer of holes from MoS<sub>2</sub> to ReS<sub>2</sub>. To observe this process, we excite the heterostructure sample with a  $76 \mu\text{J cm}^{-2}$  and 672-nm pump pulse, and probe the ReS<sub>2</sub> layer of the heterostructure with an 820-nm probe. Figures 5(a) and 5(b) show the differential reflection signal in long and short time ranges, respectively. Since the experimental conditions are identical to the measurement of the individual ReS<sub>2</sub> monolayer, as shown in Fig. 3(b), the two samples can be directly compared. We find that the signal from the heterostructure is about 3 times higher than the monolayer ReS<sub>2</sub>. For the MoS<sub>2</sub>-ReSe<sub>2</sub> heterostructure, the pump excites electrons and holes in both layers. Since electrons excited in ReS<sub>2</sub> transfer to MoS<sub>2</sub>, if holes do not transfer from MoS<sub>2</sub> to ReS<sub>2</sub>, the carrier population in ReS<sub>2</sub> of the heterostructure would be lower than that of the individual ReS<sub>2</sub>, and hence the signal would be smaller. Therefore, the observed increase of the signal in the heterostructure shows that holes can transfer from MoS<sub>2</sub> to ReS<sub>2</sub>. The decay of the signal from the heterostructure can be fit by a bi-exponential function, as indicated by the red line in Fig. 5(a), with time constants of about 1.5 and 34 ps, respectively. The short time constant could be associated with cooling of hot holes. Note that in this measurement the probe is not tuned to the excitonic resonance of ReSe<sub>2</sub>, and hence is not expected to be sensitive to the exciton formation process. However, since holes transfer to ReSe<sub>2</sub> with large energy, their energy relaxation from the states being probed to the top of the valence band causes a decrease of the signal. The long time constant reflects the lifetime of the carriers, which is about twice longer than of individual monolayer ReSe<sub>2</sub>. Similarly, the extended lifetime can be attributed to the separation of electrons and holes due to charge transfer.

In this configuration to study hole transfer, we intend to excite MoS<sub>2</sub> with the 670-nm pump. However, since ReS<sub>2</sub> has a smaller bandgap, the pump also excites ReS<sub>2</sub>. Therefore, the 820-nm probe senses holes that could be either injected directly in ReS<sub>2</sub> or transferred from MoS<sub>2</sub>. To separate the two contributions, and thus further confirm existence of hole transfer, we studied how the signal changes when we tune the pump wavelength around the optical bandgap of MoS<sub>2</sub>. The results are plotted in Fig. 5(c) along with the PL spectrum of MoS<sub>2</sub> for comparison. The strong dependence shows clearly the important role of the transferred holes, since the carrier density excited in ReSe<sub>2</sub> is not expected to have a strong dependence on the pump wavelength in this small range. In particular, when the pump wavelength is significantly longer than the PL peak energy, the signal is about  $1.2 \times 10^{-4}$ . This can be viewed as the contribution from the holes excited in ReSe<sub>2</sub> since the MoS<sub>2</sub> is not excited. At shorter pump wavelengths that can excite MoS<sub>2</sub>, the signal reaches to about  $3 \times 10^{-4}$ , due to the additional contribution to the hole population in ReS<sub>2</sub> from the transfer.

#### 4. Conclusions

We have studied charge transfer in a van der Waals heterostructure composed of monolayers of MoS<sub>2</sub> and ReSe<sub>2</sub>. Transient absorption measurements show strong evidence of ultrafast electron transfer from ReS<sub>2</sub> to MoS<sub>2</sub> and hole transfer from MoS<sub>2</sub> to ReS<sub>2</sub>. These results show that the band alignment of this heterostructure is type-II with the conduction band minimum located in MoS<sub>2</sub> and valence band maximum in ReS<sub>2</sub>. Separation of electrons and holes in different layers prolonged their recombination lifetime. These results introduce ReSe<sub>2</sub> as a new building block to construct van der Waals heterostructure with good charge transfer properties, which can be used in electronic and optoelectronic devices.

#### Funding

National Key R&D Program of China (2016YFA0202302), the National Natural Science Foundation of China (61527817, 61875236), Initiative Postdocs Supporting Program of China (BX201600013), General Financial Grant from the China Postdoctoral Science Foundation (2017M610756), Overseas Expertise Introduction Center for Discipline Innovation, 111 Center of China, and National Science Foundation of USA (DMR-1505852).

#### References

1. K. S. Novoselov, A. K. Geim, S. V. Morozov, D. Jiang, Y. Zhang, S. V. Dubonos, I. V. Grigorieva, and A. A. Firsov, "Electric field effect in atomically thin carbon films," *Science* **306**(5696), 666–669 (2004).
2. Z. Yin, H. Li, H. Li, L. Jiang, Y. Shi, Y. Sun, G. Lu, Q. Zhang, X. Chen, and H. Zhang, "Single-layer MoS<sub>2</sub> phototransistors," *ACS Nano* **6**(1), 74–80 (2012).
3. S. Cui, H. Pu, S. A. Wells, Z. Wen, S. Mao, J. Chang, M. C. Hersam, and J. Chen, "Ultrahigh sensitivity and layer-dependent sensing performance of phosphorene-based gas sensors," *Nat. Commun.* **6**(1), 8632 (2015).
4. O. Lopez-Sanchez, D. Lembke, M. Kayci, A. Radenovic, and A. Kis, "Ultrasensitive photodetectors based on monolayer MoS<sub>2</sub>," *Nat. Nanotechnol.* **8**(7), 497–501 (2013).
5. M. L. Tsai, S. H. Su, J. K. Chang, D. S. Tsai, C. H. Chen, C. I. Wu, L. J. Li, L. J. Chen, and J. H. He, "Monolayer MoS<sub>2</sub> heterojunction solar cells," *ACS Nano* **8**(8), 8317–8322 (2014).
6. J. M. Yun, Y. J. Noh, C. H. Lee, S. I. Na, S. Lee, S. M. Jo, H. I. Joh, and D. Y. Kim, "Exfoliated and partially oxidized MoS<sub>2</sub> nanosheets by one-pot reaction for efficient and stable organic solar cells," *Small* **10**(12), 2319–2324 (2014).
7. E. Gourmelon, O. Lignier, H. Hadouda, G. Couturier, J. C. Bernede, J. Tedd, J. Pouzet, and J. Salardenne, "MS<sub>2</sub> (M=W, Mo) photosensitive thin films for solar cells," *Sol. Energy Mater. Sol. Cells* **46**(2), 115–121 (1997).
8. B. Radisavljevic, M. B. Whitwick, and A. Kis, "Integrated circuits and logic operations based on single-layer MoS<sub>2</sub>," *ACS Nano* **5**(12), 9934–9938 (2011).
9. B. W. H. Baugher, H. O. H. Churchill, Y. Yang, and P. Jarillo-Herrero, "Optoelectronic devices based on electrically tunable p-n diodes in a monolayer dichalcogenide," *Nat. Nanotechnol.* **9**(4), 262–267 (2014).
10. R. Cheng, S. Jiang, Y. Chen, Y. Liu, N. Weiss, H. C. Cheng, H. Wu, Y. Huang, and X. Duan, "Few-layer molybdenum disulfide transistors and circuits for high-speed flexible electronics," *Nat. Commun.* **5**(1), 5143 (2014).
11. K. K. Kam and B. A. Parkinson, "Detailed photocurrent spectroscopy of the semiconducting group-VI transition-metal dichalcogenides," *J. Phys. Chem.* **86**(4), 463–467 (1982).
12. K. F. Mak, C. Lee, J. Hone, J. Shan, and T. F. Heinz, "Atomically thin MoS<sub>2</sub>: a new direct-gap semiconductor,"

- Phys. Rev. Lett. **105**(13), 136805 (2010).
13. H. Zhao, J. B. Wu, H. X. Zhong, Q. S. Guo, X. M. Wang, F. N. Xia, L. Yang, P. H. Tan, and H. Wang, "Interlayer interactions in anisotropic atomically thin rhenium diselenide," *Nano Res.* **8**(11), 3651–3661 (2015).
  14. D. Wolverson, S. Crampin, A. S. Kazemi, A. Ilie, and S. J. Bending, "Raman spectra of monolayer, few-layer, and bulk  $\text{ReSe}_2$ : an anisotropic layered semiconductor," *ACS Nano* **8**(11), 11154–11164 (2014).
  15. S. Yang, S. Tongay, Y. Li, Q. Yue, J. B. Xia, S. S. Li, J. Li, and S. H. Wei, "Layer-dependent electrical and optoelectronic responses of  $\text{ReSe}_2$  nanosheet transistors," *Nanoscale* **6**(13), 7226–7231 (2014).
  16. A. L. Elías, N. Perea-López, A. Castro-Beltrán, A. Berkdemir, R. Lv, S. Feng, A. D. Long, T. Hayashi, Y. A. Kim, M. Endo, H. R. Gutiérrez, N. R. Pradhan, L. Balicas, T. E. Mallouk, F. López-Urías, H. Terrones, and M. Terrones, "Controlled synthesis and transfer of large-area  $\text{WS}_2$  sheets: from single layer to few layers," *ACS Nano* **7**(6), 5235–5242 (2013).
  17. A. Arora, J. Noky, M. Drüppel, B. Jariwala, T. Deilmann, R. Schneider, R. Schmidt, O. Del Pozo-Zamudio, T. Stiehm, A. Bhattacharya, P. Krüger, S. Michaelis de Vasconcellos, M. Röhlfing, and R. Bratschkitsch, "Highly anisotropic in-plane excitons in atomically thin and bulk like  $1T'$ - $\text{ReSe}_2$ ," *Nano Lett.* **17**(5), 3202–3207 (2017).
  18. S. Yang, C. Wang, H. Sahin, H. Chen, Y. Li, S. S. Li, A. Suslu, F. M. Peeters, Q. Liu, J. Li, and S. Tongay, "Tuning the optical, magnetic, and electrical properties of  $\text{ReSe}_2$  by nanoscale strain engineering," *Nano Lett.* **15**(3), 1660–1666 (2015).
  19. D. B. Seley, M. Nath, and B. A. Parkinson, " $\text{ReSe}_2$  nanotubes synthesized from sacrificial templates," *J. Mater. Chem.* **19**(11), 1532–1534 (2009).
  20. K. Friemelt, M. C. Luxsteiner, and E. Bucher, "Optical properties of the layered transition-metal-dichalcogenide  $\text{ReS}_2$ : anisotropy in the van der Waals plane," *J. Appl. Phys.* **74**(8), 5266–5268 (1993).
  21. C. H. Ho and C. E. Huang, "Optical property of the near band-edge transitions in rhenium disulfide and diselenide," *J. Alloys Compd.* **383**(1-2), 74–79 (2004).
  22. A. K. Geim and I. V. Grigorieva, "Van der Waals heterostructures," *Nature* **499**(7459), 419–425 (2013).
  23. Y. Liu, N. O. Weiss, X. Duan, H. Cheng, Y. Huang, and X. Duan, "Van der Waals heterostructures and devices," *Nat. Rev. Mater.* **1**(9), 16042 (2016).
  24. K. S. Novoselov, A. Mishchenko, A. Carvalho, and A. H. Castro Neto, "2D materials and van der Waals heterostructures," *Science* **353**(6298), aac9439 (2016).
  25. P. Rivera, J. R. Schaibley, A. M. Jones, J. S. Ross, S. Wu, G. Aivazian, P. Klement, K. Seyler, G. Clark, N. J. Ghimire, J. Yan, D. G. Mandrus, W. Yao, and X. Xu, "Observation of long-lived interlayer excitons in monolayer  $\text{MoSe}_2$ - $\text{WSe}_2$  heterostructures," *Nat. Commun.* **6**(1), 6242 (2015).
  26. C. H. Lee, G. H. Lee, A. M. van der Zande, W. Chen, Y. Li, M. Han, X. Cui, G. Arefe, C. Nuckolls, T. F. Heinz, J. Guo, J. Hone, and P. Kim, "Atomically thin p-n junctions with van der Waals heterointerfaces," *Nat. Nanotechnol.* **9**(9), 676–681 (2014).
  27. H. M. Hill, A. F. Rigosi, K. T. Rim, G. W. Flynn, and T. F. Heinz, "Band alignment in  $\text{MoS}_2$ / $\text{WS}_2$  transition metal dichalcogenide heterostructures probed by scanning tunneling microscopy and spectroscopy," *Nano Lett.* **16**(8), 4831–4837 (2016).
  28. B. Miller, A. Steinhoff, B. Pano, J. Klein, F. Jahnke, A. Holleitner, and U. Wurstbauer, "Long-lived direct and indirect interlayer excitons in van der Waals heterostructures," *Nano Lett.* **17**(9), 5229–5237 (2017).
  29. J. S. Ross, P. Rivera, J. Schaibley, E. Lee-Wong, H. Yu, T. Taniguchi, K. Watanabe, J. Yan, D. Mandrus, D. Cobden, W. Yao, and X. Xu, "Interlayer exciton optoelectronics in a 2D heterostructure p-n junction," *Nano Lett.* **17**(2), 638–643 (2017).
  30. K. L. Seyler, P. Rivera, H. Yu, N. P. Wilson, E. L. Ray, D. G. Mandrus, J. Yan, W. Yao, and X. Xu, "Signatures of moiré-trapped valley excitons in  $\text{MoSe}_2$ / $\text{WSe}_2$  heterobilayers," *Nature* **567**(7746), 66–70 (2019).
  31. F. Ceballos, M. Z. Bellus, H. Y. Chiu, and H. Zhao, "Probing charge transfer excitons in a  $\text{MoSe}_2$ - $\text{WS}_2$  van der Waals heterostructure," *Nanoscale* **7**(41), 17523–17528 (2015).
  32. F. Ceballos, M. Z. Bellus, H. Y. Chiu, and H. Zhao, "Ultrafast charge separation and indirect exciton formation in a  $\text{MoS}_2$ - $\text{MoSe}_2$  van der Waals heterostructure," *ACS Nano* **8**(12), 12717–12724 (2014).
  33. X. Hong, J. Kim, S. F. Shi, Y. Zhang, C. Jin, Y. Sun, S. Tongay, J. Wu, Y. Zhang, and F. Wang, "Ultrafast charge transfer in atomically thin  $\text{MoS}_2$ / $\text{WS}_2$  heterostructures," *Nat. Nanotechnol.* **9**(9), 682–686 (2014).
  34. K. Wang, B. Huang, M. Tian, F. Ceballos, M. W. Lin, M. Mahjouri-Samani, A. Boulesbaa, A. A. Piretzky, C. M. Rouleau, M. Yoon, H. Zhao, K. Xiao, G. Duscher, and D. B. Geohegan, "Interlayer coupling in twisted  $\text{WSe}_2$ / $\text{WS}_2$  bilayer heterostructures revealed by optical spectroscopy," *ACS Nano* **10**(7), 6612–6622 (2016).
  35. F. Ceballos and H. Zhao, "Ultrafast laser spectroscopy of two-dimensional materials beyond graphene," *Adv. Funct. Mater.* **27**(19), 1604509 (2017).
  36. M. Li, M. Z. Bellus, J. Dai, L. Ma, X. Li, H. Zhao, and X. C. Zeng, "A type-I van der Waals heterobilayer of  $\text{WSe}_2$ / $\text{MoTe}_2$ ," *Nanotechnology* **29**(33), 335203 (2018).
  37. A. Splendiani, L. Sun, Y. Zhang, T. Li, J. Kim, C. Y. Chim, G. Galli, and F. Wang, "Emerging photoluminescence in monolayer  $\text{MoS}_2$ ," *Nano Lett.* **10**(4), 1271–1275 (2010).
  38. F. Ceballos, Q. Cui, M. Z. Bellus, and H. Zhao, "Exciton formation in monolayer transition metal dichalcogenides," *Nanoscale* **8**(22), 11681–11688 (2016).
  39. P. Steinleitner, P. Merkl, P. Nagler, J. Mornhinweg, C. Schüller, T. Korn, A. Chernikov, and R. Huber, "Direct observation of ultrafast exciton formation in a monolayer of  $\text{WSe}_2$ ," *Nano Lett.* **17**(3), 1455–1460 (2017).